UC San Diego

UC San Diego Previously Published Works

Title

Scale selection and feedback loops for patterns in drift wave-zonal flow turbulence

Permalink

https://escholarship.org/uc/item/2n71w70m

Journal

Plasma Physics and Controlled Fusion, 61(10)

ISSN

0741-3335

Authors

Guo, Weixin
Diamond, Patrick H
Hughes, David W
et al.

Publication Date

2019-10-01

DOI

10.1088/1361-6587/ab3831

Peer reviewed

eScholarship.org Powered by the California Digital Library
University of California

AUTHOR SUBMITTED MANUSCRIPT - PPCF-102471
Published as: PPCF 61, 105002 (2019)
doi:10.1088/1361-6587/ab3831

Scale selection and feedback loops for patterns in drift wave-zonal flow turbulence

Weixin Guo[1], Patrick. H. Diamond[2, 3, a], David W. Hughes[4], Lu Wang[1] and Arash Ashourvan[5]

[1]International Joint Research Laboratory of Magnetic Confinement Fusion and Plasma Physics, State Key Laboratory of Advanced Electromagnetic Engineering and Technology, School of Electrical and Electronic Engineering, Huazhong University of Science and Technology, Wuhan 430074, China.

[2]Center for Astrophysics and Space Sciences, University of California San Diego, La Jolla, California 92093, USA.

[3]Center for Fusion Science, Southwestern Institute of Physics, Chengdu, Sichuan 610041, China.

[4]Department of Applied Mathematics, University of Leeds, Leeds LS2 9JT, United Kingdom.

[5]Princeton Plasma Physics Laboratory, PO Box 451, Princeton, New Jersey 08543, USA

E-mail: pdiamond@ucsd.edu wxguo@hust.edu.cn

Abstract

The scale selection and feedback loops for the formation and sustainment of a mesoscopic staircase profile structure are investigated for drift wave-zonal flow turbulence. A mean field model derived from the Hasegawa-Wakatani system and including the evolution of mean density, mean vorticity and perturbed potential enstrophy (PE), is used. It is found that a quasi-periodic zonal staircase forms from self-sharpening of modulation. The principle feedback loop is through the nonlinear dependence of mixing length on electron density gradient, which enters by way of the potential vorticity (PV) gradient. Counterintuitively, $\vec{E} \times \vec{B}$ shearing is not effective. Moreover, the number of steps in the staircase is sensitive to both the drive (production rate of PE and initial density gradient) and damping (flow viscosity and collisional diffusivity) factors. The minimal step scale is selected by competition

[a] Author to whom any correspondence should be addressed.

between the initial density gradient and diffusive dissipation. Finite turbulence spreading is necessary to form the staircase, but moderate enhancement of turbulence spreading tends to wash out the pattern. The staircase retains a memory of its initial state. Both the mean $\vec{E} \times \vec{B}$ shear and zonal shear affect the staircase evolution. A strong mean shear quenches the pattern by suppressing the drift wave turbulence. The implications of these findings are also discussed.

Key words: scale selection, feedback loop, bistable mixing, staircase, drift wave-zonal flow

1. Introduction

Confinement scaling is a central issue for magnetic fusion, as it determines what is required to meet the criteria for ignition, etc. Usually, confinement is determined by anomalous transport, which is produced by drift wave (DW) turbulence, broadly interpreted. Such turbulence is now known to be self-regulating, via the feedback of secondary fluctuations and structures, such as zonal flow (ZF) shears and corrugations on the primary instabilities. Thus, we see that confinement scaling must be linked to the dynamics of secondary patterns, and so to the associated question of secondary pattern scale selection. The latter, of course, ultimately determines the mixing length l_{mix}, the consequent effective transport coefficient $D \sim V_* l_{mix}$, and the degree of GyroBohm breaking. Here, V_* represents the diamagnetic drift velocity.

The dynamics of secondary structures have been investigated intensively during the past twenty years. However, most of these studies have been concerned with secondary onset (i.e., ZF growth), and few have addressed the question of scale [1]. The mechanism of collisionless saturation of secondaries (i.e., zonal flows) remains obscure. An interesting clue emerged from a recent L-mode, modulated electron cyclotron resonance heating (ECRH) discharge experiment on LHD [2]. This experiment observed global hysteresis in the nonlinear dependence of fluctuation intensity and heat flux on electron temperature gradient ∇T_e. We stress that no

macroscopic internal transport barrier (ITB) was observed. The hysteresis, especially that of fluctuation intensity, suggests that the saturated turbulence is bistable [3]. In turn, this leads us to the conclusion that a good working model for pattern formation in DW-ZF turbulence should contain bistable fluctuation intensity and mean fields. A natural route to such bistability is via a gradient-dependent mixing length l_{mix}, which is a key component of the model presented in this paper.

A tractable and conceptually simple model of bistable DW turbulence with mean field feedback was recently developed [4, 5] with the aim of understanding the $\vec{E} \times \vec{B}$ staircase, the structure of which is shown in figure I. A staircase is a quasi-periodic pattern of mean field and fluctuation intensity, which results from inhomogeneous mixing, steepening and consequent self-sharpening of modulations. Bistable mixing "locks in" the steepened state as depicted in figure II.

Figure I. A schematic view of $\vec{E} \times \vec{B}$ staircase.

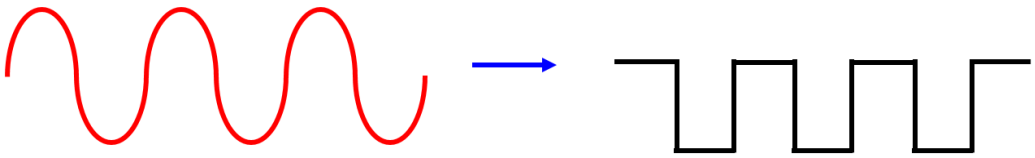

Figure II. A schematic view of bistable mixing in steepened state.

A staircase may be loosely understood by the following analogy sketched in figure III: shock is to wave as staircase is to modulation. More generally, a modulation coupled to a self-sharpening feedback loop can form a staircase structure. The signature of the staircase is the quasi-periodic array of several flat steps and sharp jumps joined by regions of large curvature (i.e., corners), as shown in figure IV. Such structures are a natural framework within which to address the scale selection problem

for saturated modulations. A characteristic scale is evident in the structure. Indeed, we advocate that one can view the staircases as a particularly clear example of a saturated DW-ZF pattern, and argue that it should be thought as a limit of a broader class of phenomena, and not as an isolated or exotic species. It is also interesting to note that simulations indicate that staircases evolve in time, albeit very slowly [6]. In particular, mergers occur, thus thinning the number of steps. Mergers happen so the system can adjust the number of steps to the boundary conditions. One should note that this process clearly departs from the conventional wisdom that the scale of the pattern is that of the fastest growing modulational instability. Indeed, the long-time step size is much larger than the scale of the initial modulation, as shown in [5].

Shock ↔ Wave
Staircase ↔ Modulation

Figure III. Analogy between shock and staircase.

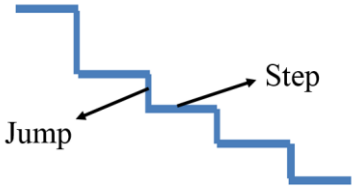

Figure IV. Jumps and steps in staircase

Staircases were first discussed in the context of mixing in stably stratified fluids [7, 8] and later in geophysical fluids [9-12]—i.e., the potential vorticity (PV) staircase, and in the context of double diffusive convection [13]. Then, they were observed in gyrokinetic simulations using GYSELA [14] and subsequently in other simulations [15-17]. There are hints of staircase structures in experiments [18, 19], though earlier experiments [20] also noted a quasi-periodic zonal pattern. Curiously, the connection between the L-mode hysteresis experiments and the zonal staircase pattern has not yet been made.

This paper focuses on studies of the mesoscopic pattern predicted by a bistable mean field model for DW turbulence in the Hasegawa-Wakatani (H-W) system. The model, which is broadly applicable, evolves fluctuation potential enstrophy (PE, proportional to fluctuation intensity), mean density and mean flow vorticity (proportional to zonal shear, in view of symmetry). Bistability enters via a gradient dependent mixing length l_{mix}, which is determined by two scales, an excitation scale

and the Rhines scale $l_{Rh} = \sqrt{\varepsilon}/|\partial_x\langle n-u\rangle|$, where ε represents the fluctuation PE, and $\partial_x\langle n-u\rangle$ is the mean PV gradient with $\langle n\rangle$ and $\langle u\rangle$ being the mean density and mean vorticity, respectively. Here, *x* denotes the radial direction. The Rhines scale, typically larger than the excitation scale, is a dynamical scale, defined by the balance of the eddy decorrelation rate and the wave mismatch frequency. Of course, here the wave frequency is set by the diamagnetic frequency, including the zonal potential, i.e., $\nabla(\langle n\rangle - \rho_s^2\partial_r^2\langle\phi\rangle)$. (Here, $\rho_s = c_s/\Omega_{ci}$ is the ion sound radius, $c_s = \sqrt{T_e/m_i}$ and $\Omega_{ci} = eB/(cm_i)$ are the sound velocity and ion cyclotron frequency, respectively, T_e is the electron temperature, m_i is the ion mass, e is the elementary charge, B is the total magnetic field, c is the velocity of light.) Here, $\nabla(\langle n\rangle - \rho_s^2\partial_r^2\langle\phi\rangle)$ is the mean PV gradient. For $k_{//}^2 v_{the}^2/\omega_r\nu_{ei}$>1, i.e., the regime most relevant to experiments ($k_{//}$ is the parallel wavenumber, v_{the} is the electron thermal velocity, ω_r is the real frequency of the eigenmode, ν_{ei} is collisional frequency), the density response of electrons is laminar, so the mean particle flux is diffusive. The vorticity flux is equivalent to the Reynolds force, via the Taylor identity [21]—and consists of mixing of both vorticity and a non-diffusive contribution (~residual stress). Furthermore, fluctuation intensity evolution includes turbulence spreading [22]. Further details of the reduced H-W model may be found in [23, 24] and in section II. The model in the present work is similar to that of [4, 5], but this paper presents a more extensive study of results and their implications.

While previous work explored and illustrated several aspects of the pattern structure, many questions were left partially or totally un-answered. In this paper, we thus focus on these questions. These include:

i). What is the principal feedback loop? Is there a preferred or dominant feedback mechanism, which defines the pattern and staircase? In particular, does the conventional wisdom that zonal $\vec{E}\times\vec{B}$ shearing is the relevant feedback mechanism apply?

ii). How do we understand parameter sensitivity? Even in a very simplified

system like H-W, many parameters enter. These include flow viscosity, collisional diffusion, growth of the drive, initial density gradient, etc. Among these, which have the most direct and important influence on the formation and sustainment of the staircase, and why? How do the parameters affect the number of steps (N_s), and thus the mean step size and the characteristic scale $\Delta r_s \sim L/N_s$, where L is the system size. Note that the scalings and dependences of N_s are crucial here, as they determine the zonal pattern scale.

iii). What are the effects of turbulence spreading? What do the effects of turbulence spreading indicate about how the staircase might respond to an avalanche?

iv). Initial conditions—i.e., does the pattern retain a memory of its initial scale?

v). Effects of mean and zonal shearing—i.e., how does mean $\vec{E} \times \vec{B}$ shear affect the zonal pattern? In a related vein, how is the staircase pattern related to macroscopic transport barrier formation, I mode with high β_N [25, 26] or quiescent H-mode (QH-mode) [27-30]?

In the present paper, we address these five questions. Although there is an unavoidable tendency to focus on "staircases", in particular, we try to elucidate the more general question of pattern scale selection in the course of this discussion.

The remainder of this paper is organized as follow. The nonlinear reduced model is presented in section 2. The pattern structure is studied in detail in section 3. In particular, subsection 3.1 explores parameter sensitivity while subsection 3.2 examines feedback loop physics via comparison of bistability via the Rhines scale mechanism with bistability via $\vec{E} \times \vec{B}$ shearing. Subsection 3.3 explores the effects of turbulence spreading, while subsection 3.4 studies the sensitivity of staircase to the initial electron density gradient drive. Then, subsection 3.5 investigates the interaction of and competition between mean and zonal shearing. Finally, section 4 presents conclusions and discussion, including broader implications and direction for future work.

2. The nonlinear reduced model

The reduced model in our work builds on the widely used H-W equations [23], which consist of the density equation

$$\frac{dn}{dt} = -D_{\parallel}\nabla_{\parallel}^2(\phi - n) + D_c\nabla_{\perp}^2(n), \quad (1)$$

and vorticity equation

$$\frac{d}{dt}(\nabla^2\phi) = -D_{\parallel}\nabla_{\parallel}^2(\phi - n) + \mu_c\nabla_{\perp}^4\phi. \quad (2)$$

Here, n and $\nabla^2\phi$ (in the following, we denote u=$\nabla^2\phi$) are the normalized total density and vorticity, respectively. We use the standard normalization for density $n = \delta\hat{n} = \delta n/n_0$ ($n_0$is the equilibrium density), the perturbed electric potential $\phi = \delta\hat{\phi} = e\delta\phi/T_e$, $D_{\parallel} = v_{the}^2/(\nu_{ei}\rho_s c_s)$ refers to the normalized parallel collisional diffusion with $v_{the} = \sqrt{T_e/m_e}$, time is normalized to $1/\Omega_i$. D_c and μ_c are the collisional particle diffusivity and flow viscosity, respectively, which damp small scales. The total density n, as well as the vorticity u, is decomposed into a mean part and a perturbed part by taking an average over the symmetry direction. The main results in the present work follow from a mean field model describing the evolution of three quantities, i.e., the mean density $\langle n\rangle$, mean vorticity $\langle u\rangle = \langle\nabla_{\perp}^2\phi\rangle$ (therefore, mean PV $\langle q\rangle = \langle n\rangle - \langle u\rangle$) and turbulent PE. Each quantity is evolved in radial direction *x* and time *t*. The derivation of these equations is presented in detail in [4, 5]. In the following, we show the essential steps in the derivation.

From Eqs. (1) and (2), using mean field theory, we can obtain the evolution equations for mean density $\langle n\rangle$ and mean vorticity $\langle u\rangle = \langle\nabla_{\perp}^2\phi\rangle$. Then, subtracting the mean component from Eqs. (1) and (2), the equations for the perturbed density δn and perturbed vorticity δu result. Thus, the evolution equation for the turbulent PE, i.e., $\varepsilon = (\delta q)^2$, easily follows. Here, $\delta q = \delta\hat{n} - \delta\hat{u}$ is the perturbed PV. Finally, the reduced model for the present work is thus:

$$\frac{\partial}{\partial t}\langle n\rangle = \frac{\partial}{\partial x}\left(D_n \frac{\partial\langle n\rangle}{\partial x}\right) + D_c \frac{\partial^2\langle n\rangle}{\partial x^2}, \tag{3}$$

$$\frac{\partial}{\partial t}\langle u\rangle = \frac{\partial}{\partial x}\left[(D_n - \chi)\frac{\partial\langle n\rangle}{\partial x}\right] + \chi \frac{\partial^2\langle u\rangle}{\partial x^2} + \mu_c \frac{\partial^2\langle u\rangle}{\partial x^2}, \tag{4}$$

$$\frac{\partial}{\partial t}\varepsilon = \frac{\partial}{\partial x}\left(D_\varepsilon \frac{\partial\varepsilon}{\partial x}\right) + \chi\left[\frac{\partial\langle n-u\rangle}{\partial x}\right]^2 - \varepsilon_c^{-1/2}\varepsilon^{3/2} + \gamma_\varepsilon\varepsilon. \tag{5}$$

Here, x refers to the radial direction as explained previously. The quasi-linear expression for turbulent radial particle flux is

$$\Gamma = \langle \delta v_x \delta n\rangle = -D_n \frac{\partial\langle n\rangle}{\partial x} + V_{conve}, \tag{6}$$

here, D_n and V_{conve} are the turbulent particle diffusivity and convection velocity, respectively. Similarly, the vorticity flux is

$$\Pi = \langle \delta v_x \delta u\rangle = (\chi - D_n)\frac{\partial\langle n\rangle}{\partial x} - \chi\frac{\partial\langle u\rangle}{\partial x}. \tag{7}$$

Here, χ is the diffusivity coefficient of PV and represents the turbulent viscosity, and the term $(\chi - D_n)\frac{\partial\langle n\rangle}{\partial x}$ accounts for the non-diffusive (i.e., residual) vorticity flux. The PV flux is

$$\Gamma_q = \langle \delta v_x \delta q\rangle = -\chi\frac{\partial\langle q\rangle}{\partial x} \tag{8}$$

Finally, the PE flux is

$$\Gamma_\varepsilon = \langle \delta v_x \delta q^2\rangle = -D_\varepsilon\frac{\partial\varepsilon}{\partial x}. \tag{9}$$

Here, D_ε is the diffusivity coefficient of PE. These fluxes have been calculated and simplified [31]. $D_n \approx l_{mix}^2\,\varepsilon/\alpha$, and the particle convection V_{conve} is assumed to be negligible compared to D_n. The expressions of diffusivity coefficients for PV and PE are $\chi \approx c_\chi l_{mix}^2\,\varepsilon/\sqrt{\alpha^2 + a_u\langle u\rangle^2}$ and $D_\varepsilon \cong \beta l_{mix}^2\varepsilon^{1/2}$. We have used mixing length theory and phenomenological arguments to obtain the functional formulas for D_n, χ and D_ε. The physics of the mixing length l_{mix} is discussed below. The parameter $\alpha = \frac{1+k_\perp^2}{k_\perp^2}D_\parallel k_\parallel^2$ measures the parallel resistive diffusion rate with $k_\perp$ being the perpendicular wavenumber, the constant multiplier c_χ controls the strength of turbulent viscosity, $a_u\langle u\rangle^2$ in the denominator of χ reflects the effects of suppression by strong flow shear, and β represents the strength of turbulence

spreading of PE. In Eq. (5), $\varepsilon_c^{-1/2}\varepsilon^{3/2}$ is the dissipative term with $(\varepsilon/\varepsilon_c)^{1/2}$ being enstrophy dissipation rate, $\gamma_\varepsilon\varepsilon$ is the production term with γ_ε being the growth rate of turbulent PE. More detailed elaborations of Eqs. (3)-(5) can be found in [4, 5]. The present work is an extension and discusses further investigations based on these equations.

Before the main results given in the next section, we need to discuss and stress the key physical content of our reduced model.

1. Both PV (or phase space density) and PE are conserved in the H-W system up to diffusive damping and external excitation.
2. A mean field approach is used in this refined (1D) predator-prey type model, which is a common treatment of drift wave-zonal flow turbulence [32]. Thus, the ZF pattern results from the nonlinear evolution of modulational instability, which describes the growth of a test shear in a gas of waves.
3. Inhomogeneous PV mixing (not momentum mixing) acts as the positive feedback for driving the pattern and leads to nonlinear feature formation in the mean profile. Bistable mixing is crucial for the pattern formation, and is related to the negative incremental diffusion region of the *S* curve in figure V.

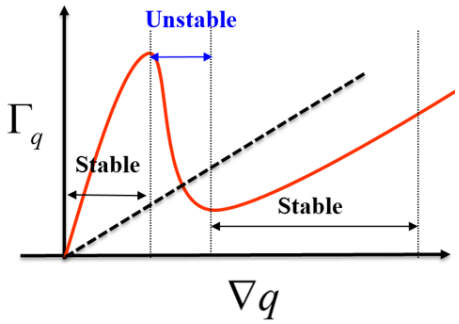

Figure V. Turbulent PV flux as a function of PV gradient.

4. Turbulence spreading is closely related to PV mixing because spreading here is simply reflected by the mixing of the intensity field.
5. The inhomogeneous PV mixing process is set by the nonlinear mixing scale l_{mix}. The dynamical feedback strongly depends on l_{mix}.
6. The nonlinear mixing length l_{mix} is a hybrid of a constant excitation scale l_0

and a dynamic length scale l_d, where l_d is usually a function of the system gradient. In [4, 5], the Rhines scale l_{Rh} has been used for l_d, so

$$l_{mix} = \frac{l_0}{\left(1+l_0^2[\partial_x(n-u)]^2/\varepsilon\right)^{\kappa/2}}, \quad (10)$$

where κ is a suppression exponent. The Rhines scale is discussed below, in point 7. Note l_{mix}~l_{Rh} for $l_{Rh} < l_0$, and l_{mix}~l_0 for $l_{Rh} > l_0$.

7. The Rhines scale emerges from the condition that the eddy turnover rate and drift wave frequency mismatch are comparable, i.e., $k_{Rh}\tilde{v} = \omega_{MM}$. The mechanism for transfer of energy from small scales to large scales changes as l_{mix} evolves from $l_{mix} < l_{Rh}$ to $l_{mix} > l_{Rh}$. In detail, for $l_{mix} < l_{Rh}$, transfer is via inverse cascade; for $l_{mix} > l_{Rh}$, transfer is via wave-zonal flow interaction. The key point for the physics of the Rhines scale mechanism can also be understood by comparing l_{mix} and l_{Rh} (shown in figure VI, where k_{Rh} is the wave number of Rhines scale). When $l_{mix} < l_{Rh}$, the turbulence is effectively a soup of eddies with short memory, so strong mixing is indicated. For $l_{mix} > l_{Rh}$, the turbulence is wave-like, memory is long and thus mixing is weak. Moreover, for $l_{mix} < l_{Rh}$, an inverse cascade carried by eddy interactions occurs. For $l_{mix} > l_{Rh}$, wave frequency exceeds the decorrelation rate, so resonant triads carry the energy. As dispersion makes satisfying the resonance condition difficult, the triads which most efficiently transfer energy are these with two drift waves and one ZF (zero frequency). Thus, the Rhines scale sets the effective ZF scale.

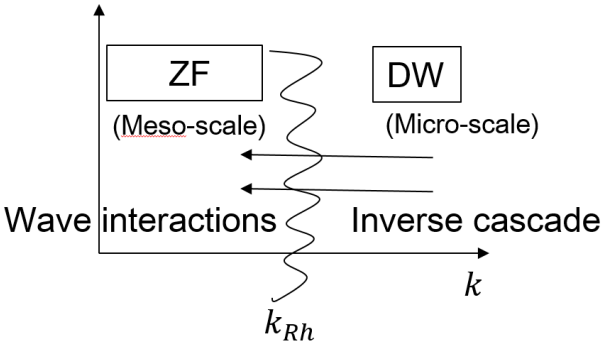

Figure VI. Key physics of Rhines scale.

8. Besides the Rhines mechanism, alternative mixing prescriptions, such as $\vec{E} \times \vec{B}$ shearing, which tilts and decorrelates the turbulent eddies as shown in figure VII,

are explored in the present work. With perpendicular shear, we have $l_{mix}^2 = \frac{l_0^2}{\left[1+\left(\bar{v}'_{E\times B}\right)^2\tau_c^2\right]^{\kappa}}$, where $\tau_c = (u^2\varepsilon/l_0^2)^{-1/4}$ is the fluctuation correlation time, $u = \bar{v}'_{E\times B}$ is the perpendicular shear rate [33]. Then, the mixing length is given by

$$l_{mix} = \frac{l_0}{\left[1+\frac{|u|}{l_0\sqrt{\varepsilon}}\right]^{\kappa/2}}. \tag{11}$$

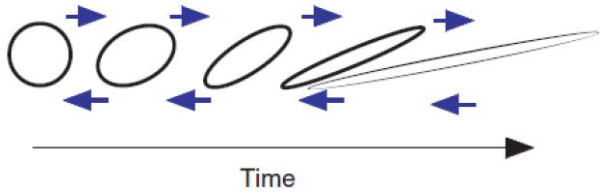

Figure VII. Variation of turbulent eddies due to $\vec{E}\times\vec{B}$ shearing.

9. For both Rhines scale and shearing mixing length, additional features of the pattern are related to the initial conditions as well as the boundary condition.

Based on these key points, we study how the scale selection and feedback loops form patterns in the drift wave-zonal flow turbulence, and explore the robustness of the pattern.

3. Model studies: numerical solutions.

In the following section, we numerically solve the nonlinear Eqs. (3)-(5), and explore how scale selection and feedback loops form the staircase structure in the DW-ZF system. The main focus is on the investigation of pattern robustness in parameter space.

The integration method is Runge-Kutta-Fehlberg, and the initial and boundary conditions for mean density n (note that $\langle ... \rangle$ is dropped to simplify the notation) and turbulent potential enstrophy ε are set, as in [5], i.e.,

$$n(x,\ t=0) = -\nabla n(t=0)\cdot x;\ n(0,t) = 0,\ n(1,\ t) = -\nabla n(t=0). \tag{12}$$

$$\varepsilon(x, t=0) = \varepsilon_i\ ;\ \varepsilon(0,t) = \varepsilon(1,\ t) = 0. \tag{13}$$

It means that a linear density profile and constant ε are initialized. For mean vorticity u (~ flow shear), we choose two different initial conditions. One is uniform flow as in [5]

$$u(x, t = 0) = 0;\ u(0, t) = u(1,\ t) = 0. \tag{14}$$

For the other case, the mean vorticity is expressed by a combination of periodic (i.e., zonal) and mean shear

$$u(x, t = 0) = Asin(N\pi x) + B;\ u(0, t) = u(1,\ t = 0) = B. \tag{15}$$

Here, A, B and $N\pi$ represent the zonal shear, mean shear and the spatial period of initial vorticity, respectively. We shall compare the results in these two different cases in section 3.2. To answer the questions i.)—v.) listed in the introduction, we use the following normalized parameters as in [5] unless otherwise stated: $\Lambda = 4000$ is the square of the ratio of macroscopic length (L) to the dynamical l_{mix}, c_χ =0.95, α=6, $D_c = \mu_c = 0.78$, $\varepsilon_c = 6.25$, $\beta = 0.1$, ε_i =0.002. The ratio of electron parallel diffusion rate to the drift wave frequency is chosen to be near adiabatic, where δn and $\nabla^2\delta\phi$ are strongly coupled, i.e., $\alpha = \frac{k_\parallel^2 V_{the}^2}{\omega\nu_{ei}} > 1$ ($\alpha \leq 1$ corresponds to the hydrodynamic region where δn and $\nabla^2\delta\phi$ tend to decouple).

3.1 Dimensionless parametric dependence of pattern structure.

In this subsection, we investigate how the dimensionless parameters affect the pattern structure by adopting the uniform flow (Eq. (14)). Scans of three parameters are studied in detail, i.e., Reynolds number $Re\sim \frac{\sqrt{\varepsilon}l^2}{\mu_c}$, Prandtl number $Pr\sim\frac{\mu_c}{D_c}$ and the ratio of production-to-dissipation ~ $\frac{\varepsilon_c\gamma_\varepsilon}{\sqrt{\varepsilon}}$. These three are chosen since:

— $Re\sim \frac{\sqrt{\varepsilon}l^2}{\mu_c}$ is a natural measure of the ratio of nonlinear transfer of enstrophy to dissipation;

— $Pr\sim\frac{\mu_c}{D_c}$ is a measure of the relative importance of dissipation in the vorticity equation and in the density equation. Pr is understood in this broader sense

rather than as a scaling parameter, in the strict sense.

— $\frac{\varepsilon_c \gamma_\varepsilon}{\sqrt{\varepsilon}}$ is a natural measure of the relative effect of growth vs dissipation.

The corresponding results are as follows.

In figure 1, we compare the density staircase and vorticity corrugation structure for $\mu_c = 0.78$ (figure 1(a), 1(c)) and $\mu_c = 1.2$ (figure 1(b), 1(d)) at time T=1. The initial density gradient is set to be $-\nabla n(t = 0) = 5.1$. We can clearly see that the number of steps (N_s) in the staircase pattern decreases with increasing μ_c. Thus, the density staircase becomes sparser, with wider steps. Similar to the density profile, the number of peaks in the corrugation pattern also decreases with flow viscosity μ_c. Since $Re \sim \frac{\sqrt{\varepsilon} l^2}{\mu_c}$, we can conclude that an increase of Re increases the number of steps. In the following sections, we focus only on expressing the trends and scaling dependences of N_s.

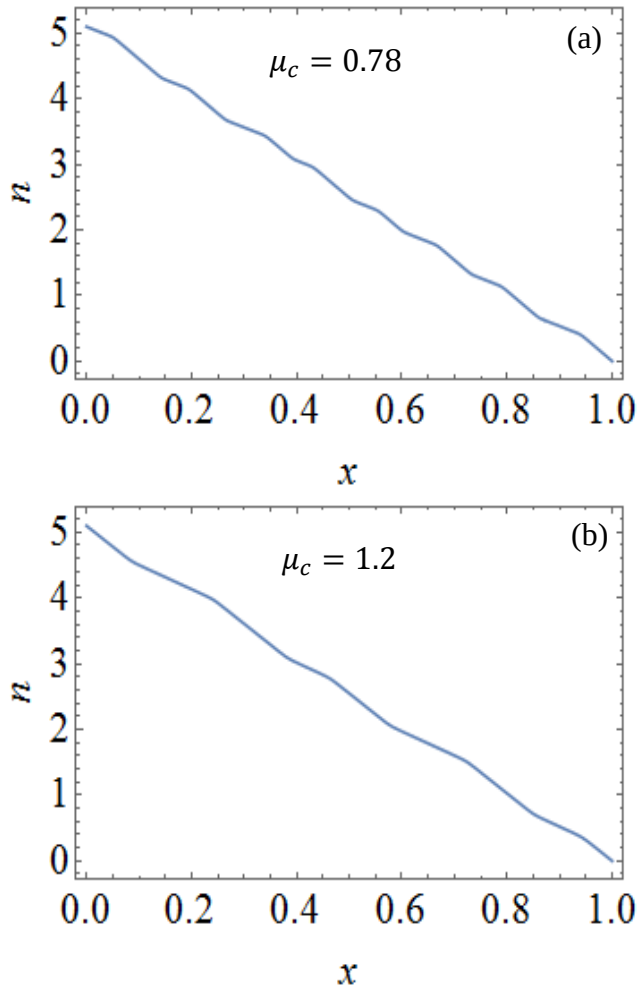

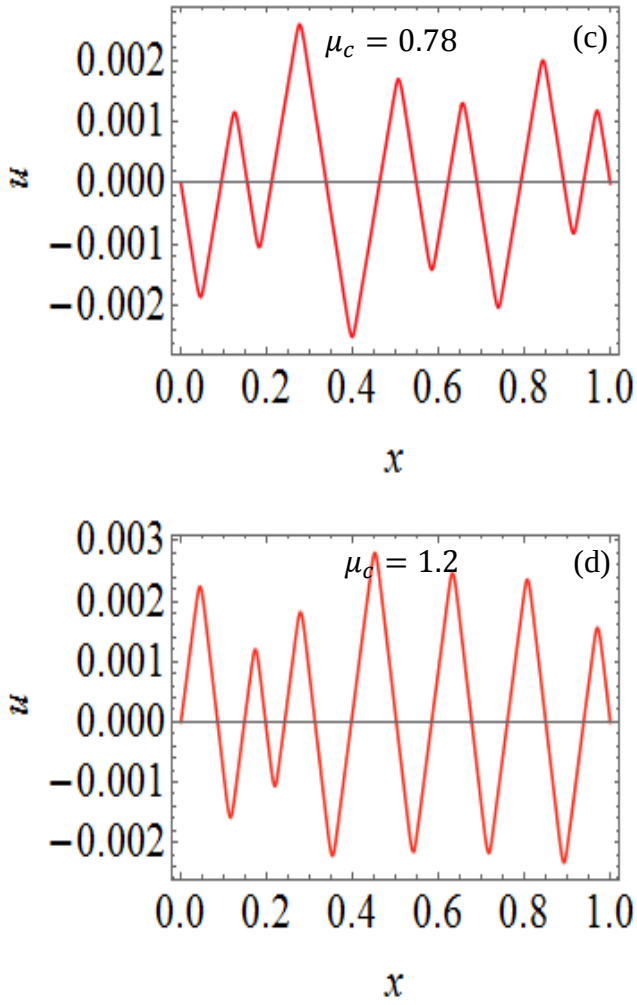

Figure 1. Mean density and mean vorticity profile at T=1. $\mu_c = 0.78$ in figure (a) and (c), and $\mu_c = 1.2$ in figure (b) and (d). The initial density gradient is $-\nabla n(t = 0) = 5.1$.

The sensitivity of patterns to $Pr \sim \frac{\mu_c}{D_c}$ is shown in figure 2. Here, we vary the particle diffusion damping coefficient D_c and keep the Reynolds number Re fixed (i.e., flow viscosity μ_c is fixed). It can be seen that N_s drops due to increasing D_c from 0.78 to 1.0. Moreover, this conclusion still holds for simultaneous variation of both D_c and μ_c. This is because the more effective impact on staircase structure is via D_c. In other words, the staircase is more sensitive to particle diffusion than to flow viscosity. We will see that increasing D_c limits ∇n steepening and its feedback through the mixing scale.

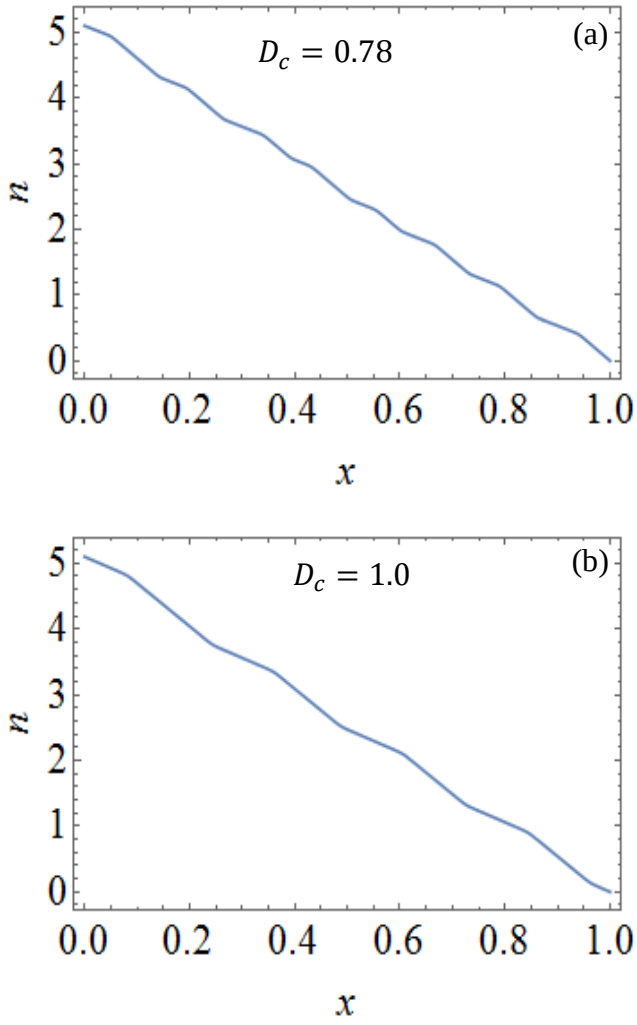

Figure 2. Mean density profile at T=1. $D_c = 0.78$ and $D_c = 1.0$ in figure (a) and figure (b), respectively. The initial density gradient is the same as figure 1, $-\nabla n(t = 0) = 5.1$.

In figure 3, we scan the ratio between the production ($P = \gamma_\varepsilon \varepsilon$) term and the dissipation ($-\varepsilon_c^{-1/2}\varepsilon^{3/2}$, where $\varepsilon_c^{-1/2}\varepsilon^{1/2}$ is enstrophy dissipation rate) term of turbulent PE presented in Eq. (5), i.e., $\frac{production}{dissipation} \sim \frac{\varepsilon_c \gamma_\varepsilon}{\sqrt{\varepsilon}}$. Figure 3(a) and 3(b) are the results with lower $\frac{\varepsilon_c \gamma_\varepsilon}{\sqrt{\varepsilon}}$ and higher $\frac{\varepsilon_c \gamma_\varepsilon}{\sqrt{\varepsilon}}$ at T=10, respectively. We see that the number of steps N_s rises by increasing $\frac{production}{dissipation}$.

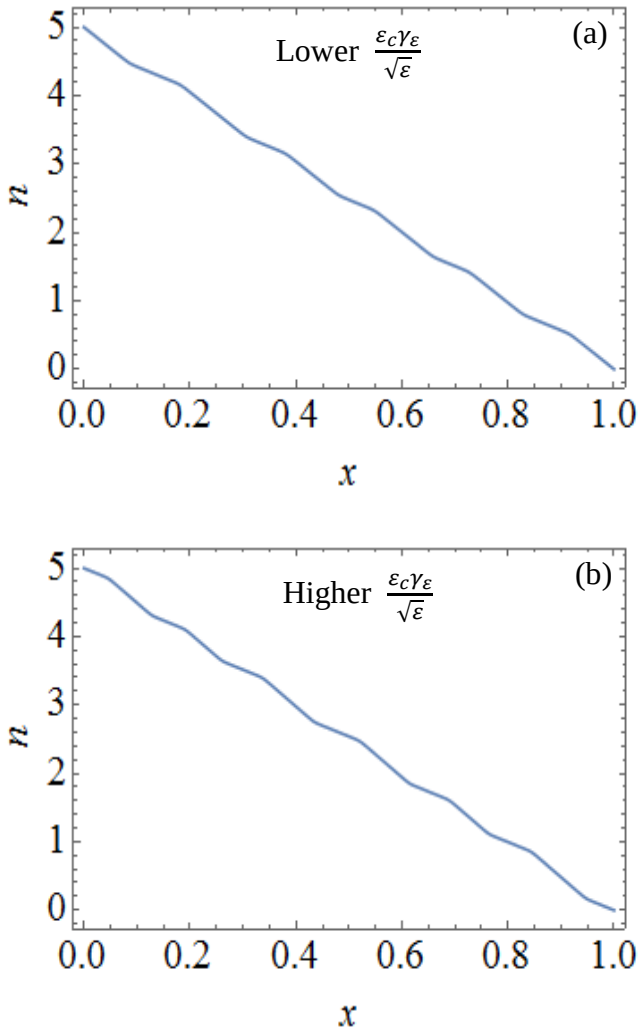

Figure 3. Mean density profile at T=10. Figure (a) and figure (b) correspond to lower $\frac{\varepsilon_c \gamma_\varepsilon}{\sqrt{\varepsilon}}$ and higher $\frac{\varepsilon_c \gamma_\varepsilon}{\sqrt{\varepsilon}}$, respectively. The initial density gradient is $-\nabla n(t=0) = 5.0$.

Combining figure 1, figure 2 and figure 3, we can easily conclude that the enhancement of drive (such as production) will increase N_s, while enhancement of damping (such as flow viscosity, particle diffusion or the dissipation) will decrease N_s. Larger values of N_s corresponds to a smaller spatial scale. Therefore, the staircase pattern will self-select the step scale (i.e., the mesoscopic scale length) in response to changing the drive or the damping. The width of step is studied in [5]. The detailed discussion of the height of the steps will be given in subsections 3.3 and 3.4.

3.2 Principal feedback loop physics

In this subsection, we focus on studying the principal feedback loop physics by comparing the results shown in figure 4 for different mixing length l_{mix}. As seen from figure 4(a), the density staircase structure disappears when we use $\vec{E} \times \vec{B}$ shearing as the main feedback process. It means that the shearing, which is equivalent here to mean vorticity u, is not an effective feedback for self-steepening. This is a surprising result that we shall discuss further.

Previous studies have suggested that the staircase structure shown in figure 4(b) exists for the feedback via the Rhines scale. This mechanism is simply that l_{Rh} decreases for steeper $\partial_x n$, thus increasing effective memory and decreasing mixing. The pattern is also sensitive to the drive and damping. Therefore, the dominant feedback must be either through the density gradient $\partial_x n$ or the vorticity gradient $\partial_x u$. To distinguish these effects, we turn off $\partial_x n$ in the expression for the Rhines scale. We see that the staircase structure does not appear, as shown in figure 4(c). This means that the nonlinear density gradient $\partial_x n$ dependence of l_{mix}, rather than the vorticity gradient $\partial_x u$ dependence, forms the *key* feedback loop. In this regard, we note that studies of turbulence near the 2/1 magnetic island in HL-2A ohmic plasmas also showed that the turbulence level is more sensitive to $\partial_x n$ than to sheared flow [34]. Our results shown are qualitatively consistent with that particular experimental finding.

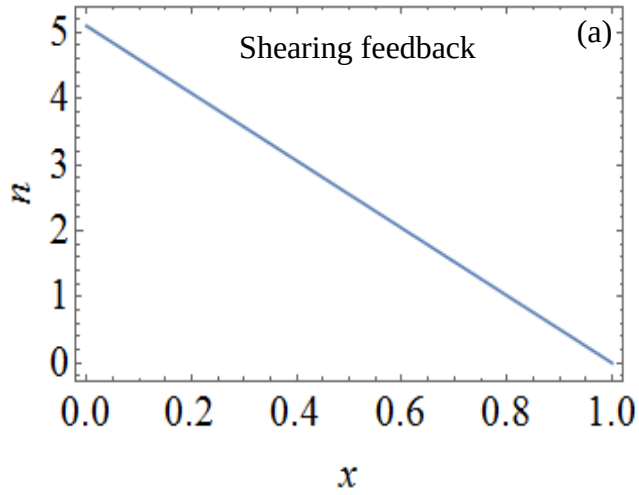

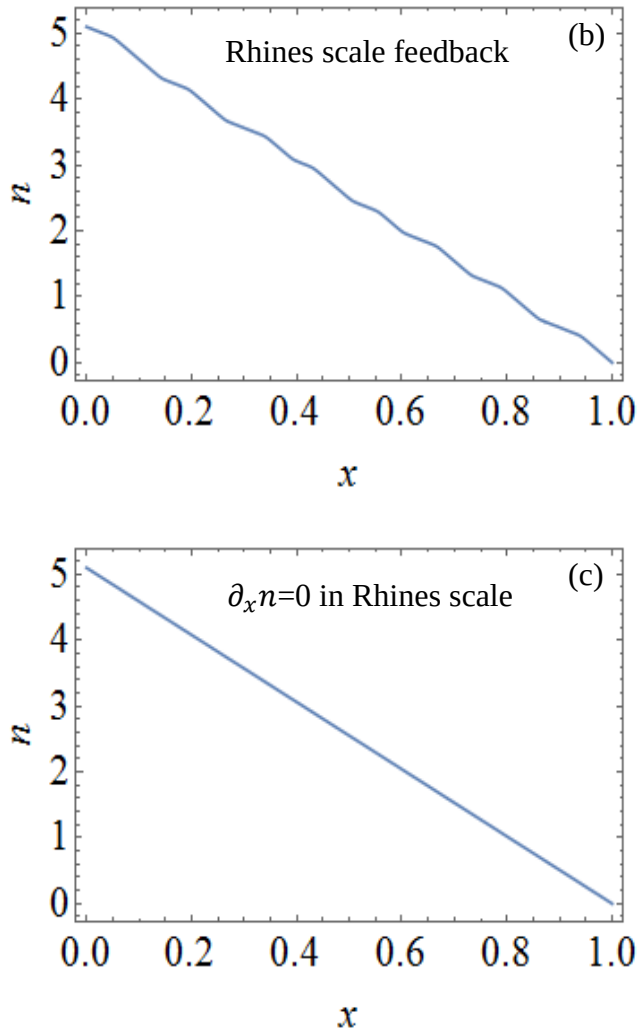

Figure 4. Mean density profile at T=1. The initial density gradient is $-\nabla n(t=0)=5.1$. Figure (a), (b) and (c) corresponds to the feedback loop through the $\vec{E}\times\vec{B}$ shearing scale (Eq. (11)), the Rhines scale (Eq. (10)) and turning off the density gradient $\partial_x n$ in the Rhines scale, respectively.

Interestingly, at the earlier stage in figure 5, for much smaller damping, we also observe that the staircase pattern appears through $\vec{E}\times\vec{B}$ shearing feedback. Here, we choose $\varepsilon(x,\,t=0)=\varepsilon(0,\,t)=\varepsilon(1,\,t)=\varepsilon_i=0.2048$, $D_c=7.8\times10^{-4}$, $\mu_c=7.8\times10^{-3}$, $\varepsilon_c=0.25$. However, the staircase pattern disappears when the system evolves for a longer time. Therefore, we see that it is difficult to sustain a stable staircase pattern through flow shearing feedback loop alone.

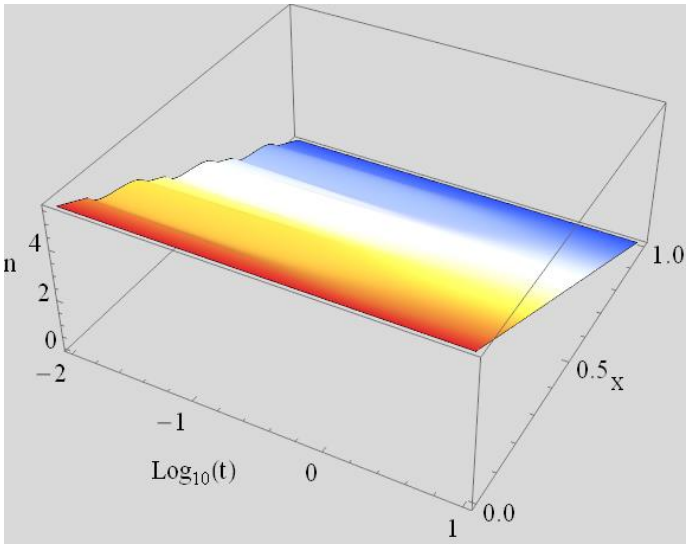

Figure 5. Evolutionary landscape of the density profile n as a function of position x and evolution time t. $\varepsilon(x,\, t=0) = \varepsilon(0,\, t) = \varepsilon(1,\, t) = \varepsilon_i$ =0.2048, $D_c = 7.8 \times 10^{-4}$, $\mu_c = 7.8 \times 10^{-3}$, $\varepsilon_c = 0.25$, and initial density gradient is $-\nabla n(t=0) = 5.6$.

3.3 Pattern sensitivity to turbulence spreading

As stated in [35], the key drive of turbulence spreading [22] is the mesoscopic inhomogeneity of the fluctuation envelope. This also enters the nonlinear dependence of l_{mix} on the PV gradient in the present paper. Thus, we also explore the response of the staircase to turbulence spreading. Here, we use the parameter β as a multiplier in the turbulent diffusivity of PE in Eq. (5), which represents complex mode interaction physics, to measure the effects of turbulence spreading of PE (proportional to fluctuation intensity). From figure 6 (a), we see that the number of steps N_s roughly decreases (i.e., larger step) with an increase of β. Therefore, the height of the step increases with β as seen in figure 6 (b). Here, we choose a narrow range of β as compared with figure 12 of [5]. We show more directly that a moderate increase in β will weaken the staircase. This is because turbulent spreading washes out small scale steps when we increase β. Thus, we conclude that the staircase pattern is sensitive to turbulence spreading, which smooths the features of small scale turbulence and thus restricts the formation of meso-scale patterns. Moreover, in figure 7, the red elliptic circles clearly show the size and height of the steps are different in

different radial position. This means an asymmetric (or non-uniform) staircase pattern is also possible for some values of β.

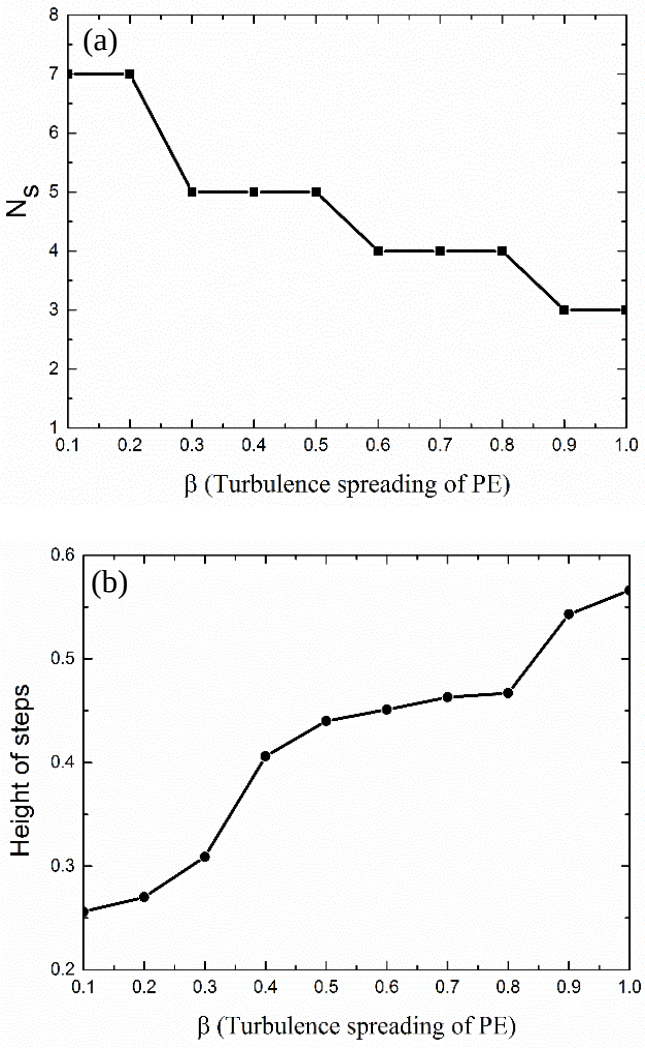

Figure 6. Number of steps N_s (figure (a)) and height of a step (figure (b)) as a function of turbulence spreading parameter β at T=1. Initial density gradient is $-\nabla n(t=0)=5.0$ and $D_c = 0.78$.

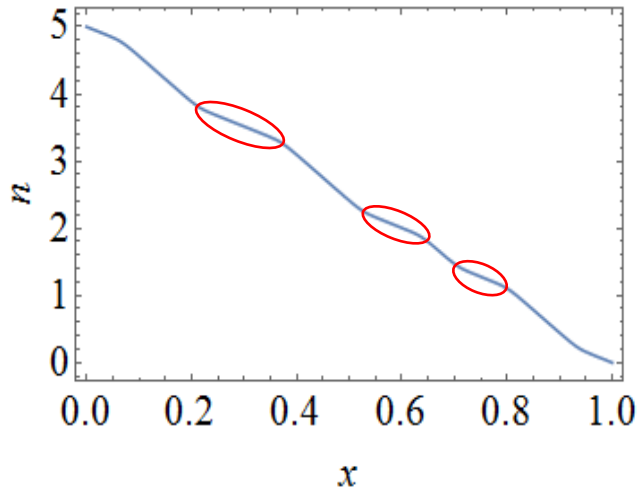

Figure 7. Mean density profile for β =0.7 at T=1. The other parameters are the same as in figure 6. The staircase exhibits irregular steps, which is highlighted.

3.4 Memory of initial conditions

The above discussions are all at fixed initial density gradient. As shown in [5], the staircase is also sensitive to the initial value of the density gradient $-\nabla n(t=0)$. Figure 8 shows the variation of the number and height of steps as a function of $-\nabla n(t=0)$. Here, we choose the different parameters as in [5], i.e., $\mu_c = 0.66, D_c = 1.2, \Lambda = 5000$. In figure 8(a), the number of steps N_s first increases and later decreases with increasing $-\nabla n(t=0)$. Thus, there must exist a minimal step scale, as shown in figure 8(b). This occurs when $-\nabla n(t=0) = 5.1$. These non-monotonic variations can be understood as follows: the initial rise in N_s and the resulting drop of the step height follow from the fact that the free energy to excite the drift wave turbulence and meso-scale pattern increases. But, the opposite effects of diffusive dissipation limit the small scales. When the system reaches its minimal step scale, dissipation is not yet very effective. A further increase in $-\nabla n(t=0)$ will in turn decrease the number of steps N_s.

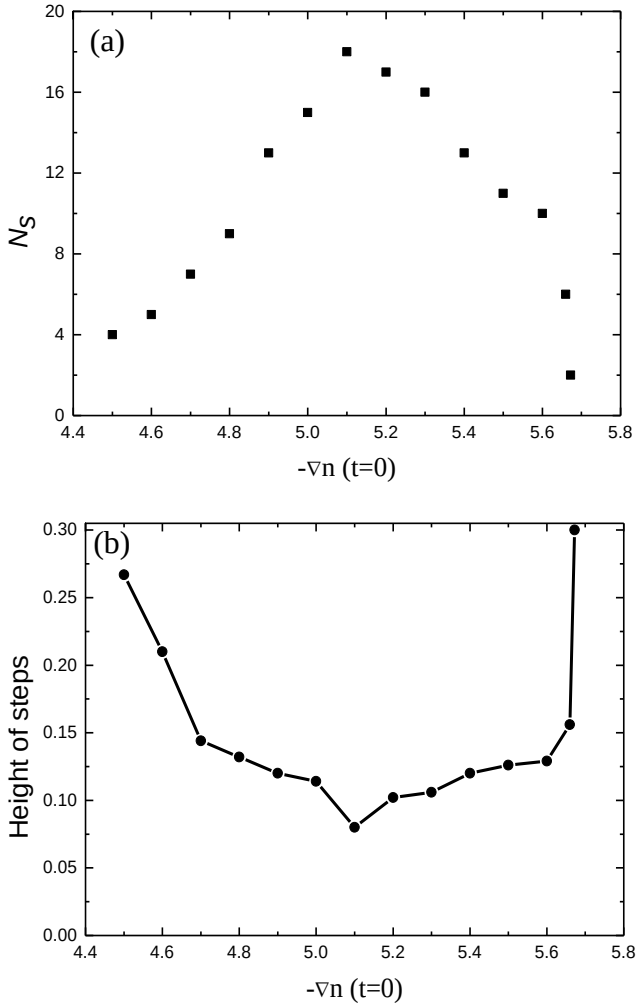

Figure 8. Variation of the number N_s (figure (a)) and height (figure (b)) of steps with initial free energy $-\nabla n(t=0)$ at T=1. The value of the parameters are $\mu_c = 0.66,\ D_c = 1.2,\ \Lambda = 5000$.

3.5 Mean ExB shear and zonal shear effects on the meso-scale pattern

In this subsection, we set the initial flow shearing (i.e., $u(x,t=0)$) as $u(x,t=0) = Asin(N\pi x) + B$ in Eq. (15), where A and B are the initial zonal shear and mean shear, respectively, and N is the mode number of the meso-scale initial condition, and represents the periodicity of u. The results are given figures 9, 10, 11 and 12 at T=10 with initial density gradient $-\nabla n(t=0) = 5.0$.

In figure 9, we explore the mean shear effects on the staircase pattern by fixing $N = 7,\ A = 0.003$ and varying B. When the mean shear is smaller than some values, such as in figures 9(a) and 9(b), we can see that the increase of mean shear does not

have a significant effect on the staircase pattern. Much stronger mean shear gradually quenches the staircase. This is because the stronger mean shear suppresses the DW turbulence, which excites the meso-scale pattern. It should be noted that the external mean shear usually has a macroscopic characteristic scale length. Thus, a self-consistent study of mean shear effects on pattern structure is needed, and is left for the future.

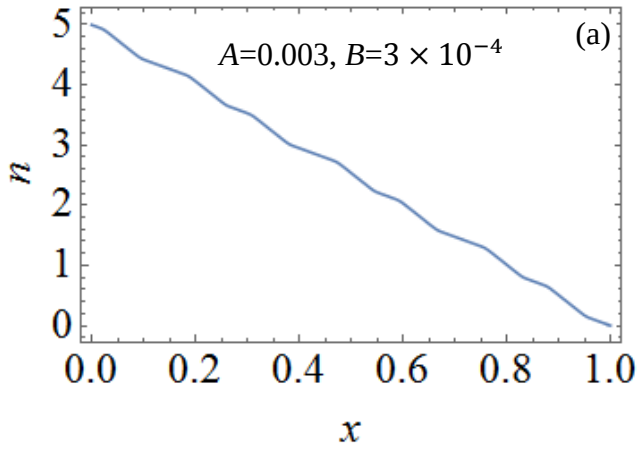

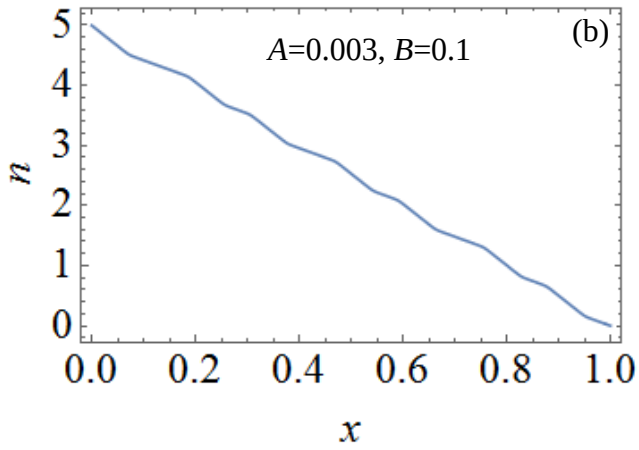

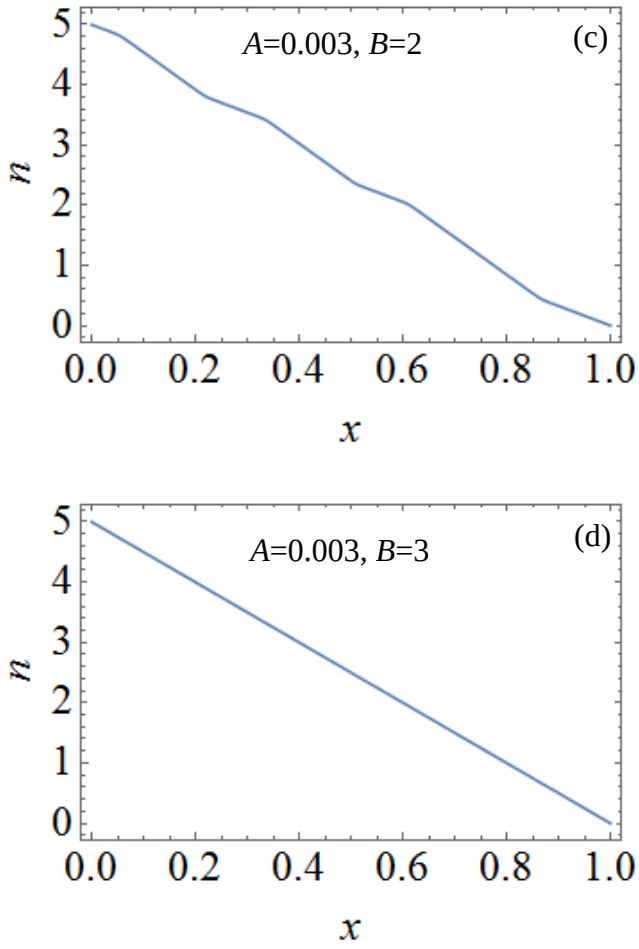

Figure 9. Mean density profiles with different values of mean shear B. Here, the fixed zonal shear is set at $A = 0.003$. Figure (a) corresponds to $B < A$, while figure (b), (c) and (d) are $B \gg A$.

Similarly, we also investigate the effects of zonal shear on the pattern. The results are shown in figure 10. Here, we fix $N = 7$, $B = 0.001$. We can see that the increase of the zonal shear component A from 10(a) to 10(b), significantly weakens the staircase and causes a decrease in the number of steps N_s. Moreover, it is not hard to infer that the staircase pattern will finally be destroyed by much stronger zonal shear, as shown in figure 9. Thus, we conclude that both mean shear and zonal feedback can influence the evolution of the staircase, and stronger shear quenches the meso-scale pattern.

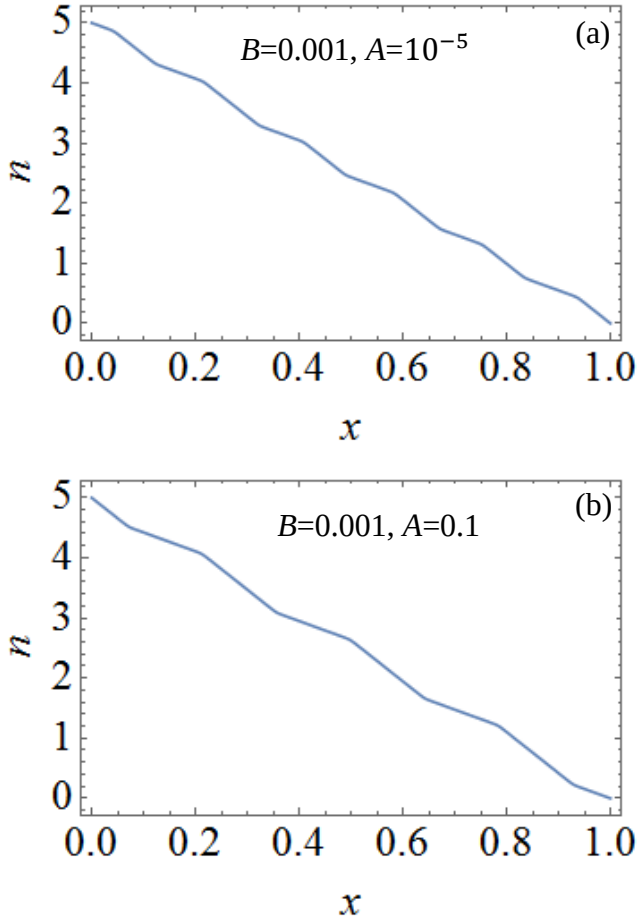

Figure 10. Mean density profiles with different values of zonal shear A. Here, mean shear B is fixed at $B = 0.001$, and the zonal shear A increases from figure (a) to (b).

Moreover, we have shown an asymmetric (non-uniform) pattern, where the size and the height of steps are different at different radial positions. It shows that this asymmetric staircase can be also formed when zonal shear is comparable to mean shear ($A = B$). In order to illustrate the non-uniform pattern more clearly, we show the height of the steps at different positions in figure 11. We see more clearly that the staircase is asymmetric.

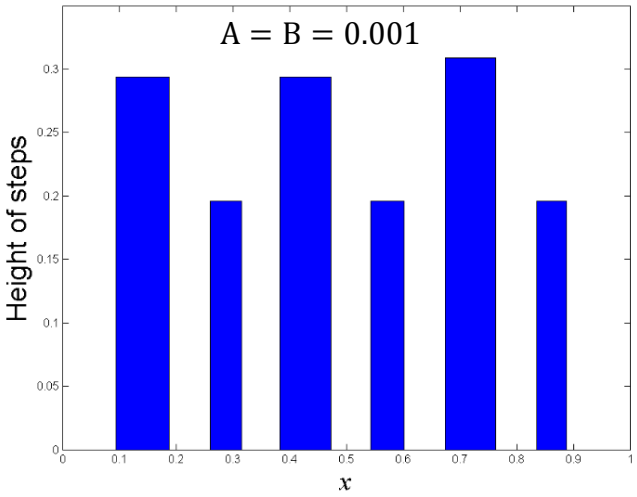

Figure 11. Variation of the height of steps in the staircase structure when mean shear and zonal shear are comparable, i.e., $A = B = 0.001$.

In figure 12, the mode number of the meso-scale initial condition of the sinusoidal shearing profile is varied while keeping fixed A and B, $A = 1$, $B = 0.001$. We can see from figure 12(a) that both the number of steps N_s (black squares) and the number of jumps N_j (red dots) increase linearly when we increase N (i.e., the periods of initial oscillation) from 1 to 12. In detail, the number of jumps (steps) increases when N increases from odd (even) to even (odd). The number of jumps will temporarily saturate when the number of steps is increasing (and vice versa). This shows that the staircase retains a strong memory of initial condition. The increase in both N_s and N_j saturates for $N = 12$. The corresponding mean density, mean vorticity and turbulent PE are shown for $N = 12$ in figures 12(b), 12(c) and 12(d), respectively. These also clearly show the existence of a staircase structure in density as well as the corrugation structure in vorticity.

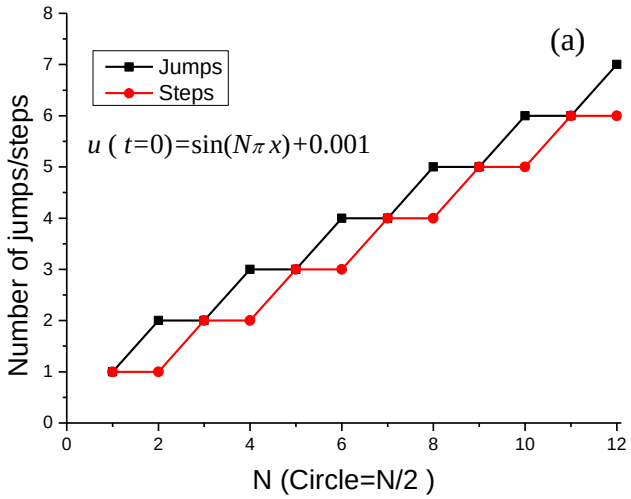
(a)
Jumps
Steps
$u\ (t=0)=\sin(N\pi x)+0.001$
Number of jumps/steps
N (Circle=N/2)

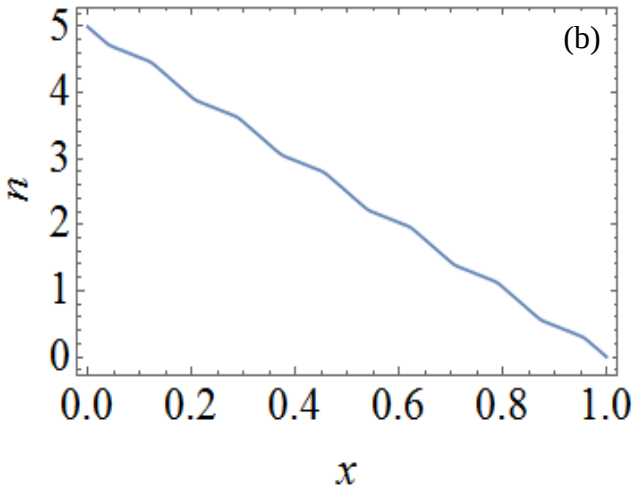
(b)
n
x

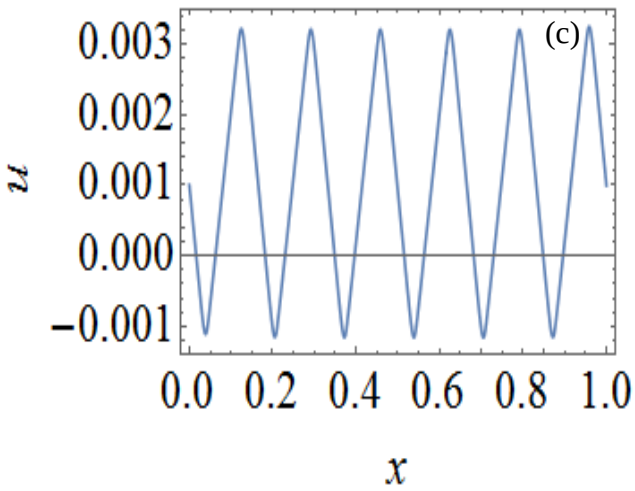
(c)
u
x

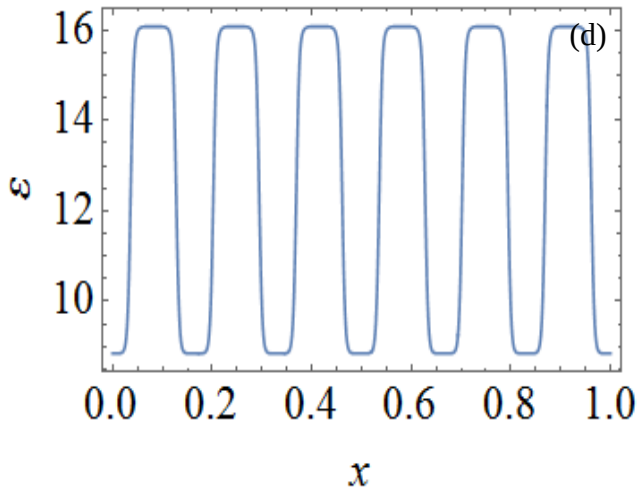

Figure 12. (a): The number of steps (black squares) and jumps (red dots) as a function of mode number N; (b), (c) and (d) are mean density, mean vorticity and turbulent PE profile, respectively.

As a short summary in this section, we have studied the robustness of staircase formation by solving the coupled nonlinear equations for mean density, mean vorticity and perturbed potential enstrophy. We have thus obtained answers to the questions listed in the introduction. The main conclusions and related discussions, as well as the implications, will be given below.

4. Conclusion and discussion

In this paper, we have studied the scale selection mechanism and feedback loop structure for drift wave-zonal flow turbulence. These studies utilized a mean field model with a bistable mixing length. The existence of the density staircase and the associated vorticity corrugations are investigated numerically, using this reduced model of the H-W system. We investigated and compared the effectiveness of feedback mechanisms that form and sustain the pattern. We also presented detailed studies of the dependence of pattern structure on both dimensionless parameters and the boundary conditions. Both are directly related to drive and damping factors. The effects of turbulence spreading as well as these of mean shear and zonal shear on the pattern are studied. The principal results of this paper are:

i). The nonlinear dependence of l_{mix} on ∇n is the key feedback mechanism

for forming and sustaining the staircase pattern. This is qualitatively consistent with the experimental results in HL-2A ohmic plasmas [34], where the level of turbulence near the 2/1 magnetic island is more sensitive to ∇n than to flow shear. The ∇n feedback works via the Rhines scale, which enters the gradient dependent mixing length. Surprisingly, zonal $\vec{E} \times \vec{B}$ shearing feedback is not effective at sustaining the structure of the pattern.

ii). The staircase pattern is affected by both the flow viscosity and particle diffusivity, and can be quenched by both of them. Not surprisingly (given the crucial role of ∇n feedback), the staircase is more sensitive to particle diffusivity than to flow viscosity. Raising the production rate (i.e., growth) of PE increases the number of steps in the staircase, and thus allows selection of a minimal step scale. Strong production reduces the effective step size ($\sim L/N_s$), which is ultimately limited by the mode correlation length. Thus, the competition between production and diffusive dissipation defines the minimum scale.

iii). Moderate turbulence spreading significantly weakens the pattern. However, some finite turbulence spreading is necessary to smooth the curvature (i.e., the corners) of the staircase structure.

iv). The staircase retains a memory of its initial pattern.

v). Both the mean shear and zonal feedback influence the evolution of the zonal pattern. Very strong $\vec{E} \times \vec{B}$ shear quenches the staircase.

From these results, we can conclude that the quasi-periodic, staircase-like structure in density (as well as in potential vorticity) is formed by self-sharpening of density modulations. This is simply inhomogeneous mixing of density. Most importantly, the principal feedback loop is through nonlinear dependence of mixing on the driving density gradient, which enters the Rhines scale. Therefore, steeper ∇n corresponds to small Rhines scale l_{Rh}, and thus to smaller mixing length l_{mix}. It then results in a smaller level of transport (i.e., smaller particle/thermal diffusivity). In turn, smaller transport is favorable for steeper ∇n, which thus closes the feedback loop, as

shown in figure VIII. $\vec{E} \times \vec{B}$ shearing feedback, as commonly assumed, does not result in the formation of non-trivial patterns. We see that the zonal pattern scale is determined by the length of the system and by the number of steps. The latter is set by ∇n, dissipation, boundary effects and turbulence spreading. The greater sensitivity to particle diffusion D_c than to flow viscosity μ_c is consistent with the dominance of ∇n feedback. The increase in step number with γ_ε (the growth rate of production) is a possible explanation of why staircases are observed only near marginality. Increasing step number drives down the step size in a fixed domain, eventually squeezing the step size into the correlation scale of the underlying turbulence.

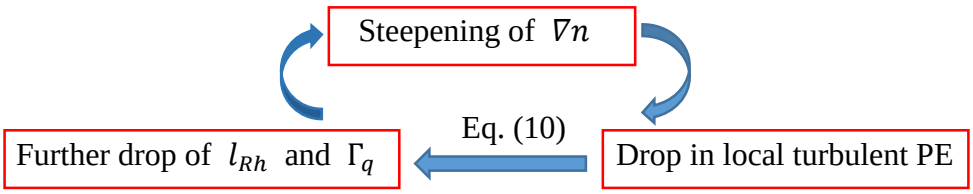

Figure VIII. A schematic view of feedback loop.

More generally, we conclude that reduced models are a useful complement to large scale simulations. A cynical reader may ask—Why bother? Of what use are simple models? Why not simply explore the staircase formation phenomenon using so-called "first principle direct numerical simulation (DNS)"? We respond by noting:

i). reduced models allow us to formulate, isolate and test different physical ideas and scenarios concerning staircase formation. They allow us to identify the roles and relative importance of competing processes;

ii). reduced models distill and clarify the message from large DNS. Indeed, if one truly has learned something from a serious of large DNS, one should be able to condense the lesson into an illustrative reduced model;

iii). reduced models are useful to guide, and analyze the results of larger scale DNS. Without such simple models, one can not extract anything useful from big simulations;

iv). most importantly, reduced models (and theoretical concepts) provide a framework for, and give meaning to experiments, both physical and digital.

This process of "modelization" is essential to conceptual progress.

This paper motivates several directions for future work. These include, but are not limited to:

i). understanding why $\vec{E} \times \vec{B}$ shearing feedback is ineffective, and also better characterizing the relation between the Rhines mechanism, scale and transport, which leads to self-sharpening,

ii). qualitative studies of parameter scans in conjunction with basic experiments,

iii). flux-driven calculations, to probe the pattern evolution and the transition between different global states of the system. These should be complemented by fundamental extensions of the basic model to encompass mean shearing effects,

iv). extensions to richer basic plasma models, beyond the H-W system,

v). a better understanding of the evolution of the zonal pattern in general. In particular, it seems possible to understand ZF in two limits, namely:

(a) the quasi-linear growth stage of modulational instability,

(b) the strongly nonlinear state of sharpened gradients, corresponding to a staircase.

One would like a clearer understanding of the transition from (a) to (b), and the conditions required for it. For example, does the transition require certain critical conditions? Likewise, one may also wonder about the ZF pattern structure if full self-sharpening does not occur. These questions require further study, beyond this paper.

The collapse of the staircase for $\vec{E} \times \vec{B}$ shearing feedback and the seeming need for feedback via ∇n are surprising results, which fly in the face of conventional wisdom. These merit further study. We remark that independent investigations reported a result that suggests ∇T_i feedback is the principal mechanism for staircase formation in ITG turbulence [15]. However, this study did not address the physics of the feedback mechanism. We note that the Rhines mechanism is generic to drift wave turbulence, though its strength varies with dispersion. Moreover, such ∇n-dependent

mixing feedback is a natural route to enhanced confinement regimes characterized by steep density gradients. In this regard, recall the results shown in figure 8(a), which scans N_s (the number of steps in staircase structure) versus $-\nabla n(t=0)$. This result shows that for a steep initial ∇n, the staircase condenses into a single, large step, which is a transport barrier by any other name! Hence, we plan to explore this feedback channel and its implications in future work. In particular, it is a candidate trigger mechanism for the L-H transition, and merits further investigation in this regard.

Acknowledgement

This work was supported by the National Key R&D Program of China under Grant No. 2017YFE0302000, the National Natural Science Foundation of China under Grant No. 11675059, the Initiative Postdocs Supporting Program of China under Grant No. BX20180105, and by U.S. Department of Energy, Office of Science, OFES under Award Number DE-FG02-04ER54738. Weixin Guo thanks UCSD for hospitality during a visit. The authors are grateful to participants in the 9th Festival de Théorie, Aix-en-Provence, France 2017, the First Chengdu Festivl, Chengdu, China 2018 and the 8th Asia Pacific Transport Working Group (APTWG), Leshan, China 2018 for discussions. We specifically acknowledge G. Dif-Pradalier, G. Tynan and J. M. Kwon, K. Ida for useful and interesting discussions. Last but not the least, we also thank G . T. Katt, Mao Midan, Mao Erbao, Larry T. Katt, Palmerston and Gladstone for inspiration during the preparation of this paper.

References

[1] Wang L, Wen T et al 2016 Nucl. Fusion 56 106017.

[2] Inagaki S, Tokuzawa T et al 2013 Nucl. Fusion 53 113006.

[3] Guo Z B and Diamond P H 2017 Phys. Plasmas 24 100705.

[4] Ashourvan A and Diamond P H 2016 Phys. Rev. E 94 051202.

[5] Ashourvan A and Diamond P H 2017 Phys. Plasmas 24 012305.

[6] Malkov M A and Diamond P H 2019 Phys. Rev. Fluids 4 044503.

[7] Phillips O M 1972 Deep Sea Research and Oceanographic Abstracts 19 79.

[8] Balmforth N J, Llewellyn Smith S G et al 1998 J. Fluid Mech. 355 329.

[9] Dritschel D G and McIntyre M E 2008 J. Atmos. Sci. 65 855.

[10] Obuse K, Takehiro S I et al 2010 Phys. Fluids 22 056601.

[11] Obuse K, Takehiro S I et al 2011 Physica D: Nonlinear Phenomena 240 1825.

[12] Obuse K, Takehiro S I et al 2012 Jpn. J. Indust. Appl. Math. 30 111.

[13] Radko T, Flanagan J D et al 2014 J. Phys. Oceanogr. 44 1285.

[14] Dif-Pradalier G, Diamond P H et al 2010 Phys. Rev. E 82 025401.

[15] Dif-Pradalier G, Hornung G et al 2017 Nucl. Fusion 57 066026.

[16] Hornung G, Dif-Pradalier G et al 2017 Nucl. Fusion 57 014006.

[17] Wang W, Kishimoto Y et al 2018 Nucl. Fusion 58 056005.

[18] Dif-Pradalier G, Hornung G et al 2015 Phys. Rev. Lett. 114 085004.

[19] Minjun J. Choi, M. H. Woo et al 2018 arXiv:1806.04947v2.

[20] Fujisawa A, Itoh K et al 2004 Phys. Rev. Lett. 93 165002.

[21] Taylor Geoffrey I and Shaw William N 1915 Philosophical Transactions of the Royal Society of London. Series A, Containing Papers of a Mathematical or Physical Character 215 1.

[22] Hahm T S, Diamond P H et al 2004 Plasma Phys. Control. Fusion 46 A323.

[23] Hasegawa A and Wakatani M 1983 Phys. Rev. Lett. 50 682.

[24] Hasegawa A and Wakatani M 1987 Phys. Rev. Lett. 59 1581.

[25] Hubbard A E, Osborne T et al 2016 Nucl. Fusion 56 086003.

[26] Whyte D G, Hubbard A E et al 2010 Nucl. Fusion 50 105005.

[27] Burrell K H, Austin M E et al 2002 Plasma Phys. Control. Fusion 44 A253.

[28] Wilks T M, Garofalo A M et al 2018 Nucl. Fusion 58 112002.

[29] Guo Z B and Diamond P H 2015 Phys. Rev. Lett. 114 145002.

[30] Brunetti D, Graves J P et al 2019 Phys. Rev. Lett. 122 155003.

[31] Ashourvan A, Diamond P H et al 2016 Phys. Plasmas 23 022309.

[32] Diamond P H, Itoh S I et al 2005 Plasma Phys. Control. Fusion 47 R35.

[33] Hajjar R J, Diamond P H et al 2018 Phys. Plasmas 25 022301.

[34] Jiang M 2018 8th Asia-Pacific Transport Working Group (APTWG) International Conference, June 12-15, 2018, Leshan, China.

[35] Hahm T S and Diamond P H 2018 J. Korean Phys. Soc. 73 747.